Journal of Electroceramics, 15, 183–192, 2005

Control of Microwave Dielectric Properties in the System $BaO \cdot Nd_2O_3 \cdot 4TiO_2$—$BaO \cdot Al_2O_3 \cdot 4TiO_2$

FERIDOON AZOUGH, TRISTAN LOWE & ROBERT FREER*

Manchester Materials Science Centre, The University of Manchester/UMIST, Grosvenor Street, Manchester, M1 7HS, UK

Submitted July 9, 2004; Revised April 19, 2005; Accepted May 20, 2005

Abstract. $BaO \cdot Nd_2O_3 \cdot 4TiO_2$—based ceramics were prepared by the mixed oxide route. Specimens were sintered at temperatures in the range 1200–1450°C. Microstructures were investigated by scanning electron microscopy (SEM) and transmission electron microscopy (TEM); microwave dielectric properties were determined at 3 GHz by the Hakki and Coleman method. Product densities were at least 95% theoretical. The addition of up to 1 wt% Al_2O_3 to the starting mixtures reduced the sintering temperatures by at least 100°C. Incorporation of small levels of Al into the structure (initially Ti sites) led to an increase in $Q \times f$ values, from 6200 to 7000 GHz, a decrease in relative permittivity (ε_r) from 88 to 78, and moved the temperature coefficient of resonant frequency (τ_f) towards zero. The addition of 0.5 wt% Al_2O_3 with 8 wt% Bi_2O_3 improved densification, increased both ε_r (to 88) and $Q \times f$ (to 8000 GHz) and moved τ_f closer to zero.

Ceramics in the system $(1-x)BaO \cdot Nd_2O_3 \cdot 4TiO_2 + xBaO \cdot Al_2O_3 \cdot 4TiO_2$ exhibited very limited solid solubility. The end member $BaO \cdot Al_2O_3 \cdot 4TiO_2$ was tetragonal in structure with the following dielectric properties: $\varepsilon_r = 35$; $Q \times f = 5000$ GHz; $\tau_f = -15$ppm/°C. Microstructures of the mixed Nd-Al compositions contained two distinct phases, Nd-rich needle-like grains and large Al-rich, lath-shaped grains. Products with near zero τ_f were achieved at compositions of approximately $0.14BaO \cdot Nd_2O_3 \cdot 4TiO_2 + 0.86BaO \cdot Al_2O_3 \cdot 4TiO_2$, where $Q \times f =$ 8200 GHz and $\varepsilon_r = 71$.

Keywords: microwave dielectric ceramics, $BaO \cdot Nd_2O_3 \cdot 4TiO_2$, $BaO \cdot Al_2O_3 \cdot 4TiO_2$

1. Introduction

The miniaturisation in microwave-based technology requires microwave dielectric ceramics with high relative permittivity (ε_r), low dielectric loss (or high Q value, usually reported in terms of $Q \times f$ where f is the resonant frequency) and near-zero temperature coefficient of resonant frequency (τ_f). Today, a wide range of materials is available with ε_r in the range 20–90 [1]. Tungsten bronze structure ceramics in the system $Ba_{(6-3x)}Nd_{(8+2x)}Ti_{18}O_{54}$ have ε_r in the upper part of the permittivity range and exhibit excellent microwave dielectric properties [1–3]. The basic structure of such compounds includes elements of the tungsten bronze framework in which corner sharing TiO_6 octahedra form networks of pentagonal, tetragonal and triangular channels. Rare earth ions preferentially occupy the rhombic channels, while Ba ions fill the pentagonal channels and any remaining Ba ions occupy the rhombic channels. The triangular channels are empty. Amongst the barium rare earth titanate compositions, compounds based on baria, neodymia and titania in a 1:1:4 ratio (ie $BaO \cdot Nd_2O_3 \cdot 4TiO_2$) have a good combination of permittivity and loss characteristics, with $\varepsilon_r = 88$ and Q.f = 6000–7000 but τ_f of +90 ppm/°C [4–6]. For commercial applications, additions of Pb and Bi have been utilised [3, 6, 7] to move τ_f close to zero. By replacing Nd by other rare earths (La, Sm, Pr) families of tungsten bronze structure ceramics have been prepared and investigated [4, 5, 8, 9]. The existence of phases with $BaO:Ln_2O_3:TiO_2$ in the ratios 1:1:3, 1:1:4, 1:1:4.5 and 1:1:5 has been debated for many years, and there still exists conflicting data

*To whom all correspondence should be addressed.
E-mail: robert. Freer@manchester.ac.uk

for details of the crystallography and extent of solid solution in many of the series [10]. However, it is clear that substitution of the rare earth ion into the structure has a dramatic effect on the properties. For example substitution of ions of increasing size (eg in the sequence Sm, Nd, Pr and La) into the rhombic channels of the tungsten bronze structure cause the Q values to decrease and the relative permittivity to increase [1]. Rather less attention has been paid to the effect of incorporating ions other than rare earths into the structure.

Mizuta et al. [11] explored the substitution of Al on Ti sites in the samarium analogue, ie the $(Ba_{6-3x}Sm_{8+2x})_\alpha Ti_{18-y}Al_yO_{54}$ system. Their object was to assess opportunities for, and the effect of substitutions on the so-called B sites. They found a solid solution existed for $y \leq 1.61$. The addition of Al tended to reduce ε_r, reduce $Q \times f$ in a non-linear way and make τ_f more negative. Mizuta et al. noted that in tungsten bronze structure materials with positive τ_f, such as $Ba_{(6-3x)}Nd_{(8+2x)}Ti_{18}O_{54}$, the incorporation of Al on the A site should bring τ_f closer to zero.

Over 30 years ago Guha and Kolar [9] explored the system $BaO \cdot Al_2O_3 \cdot TiO_2$ and identified a compound, equivalent to $BaO \cdot Al_2O_3 \cdot 4TiO_2$, having an hexagonal structure. Later, Guha et al. [12] reported the existence of $BaO \cdot Al_2O_3 \cdot 5TiO_2$ which is also hexagonal. Solomah et al. [13] confirmed the structural data for $BaO \cdot Al_2O_3 \cdot 5TiO_2$. The existence of a mineral with hollandite-type structure, having the formula $BaO \cdot Al_2O_3 \cdot 4 \cdot 5TiO_2$ has also been reported [14]. All the early investigations focussed on the synthesis and structures of powders. The dielectric properties of ceramics in the system $BaO\text{-}Al_2O_3\text{-}TiO_2$ have received minimal attention

In this study we have investigated two aspects of $Ba_{4.5}Nd_9Ti_{18}O_{54}$ ceramics. Firstly the effect of substituting small amounts of Al in $Ba_{(6-3x)}Nd_{(8+2x)}Ti_{18}O_{54}$, whilst a single phase product is maintained; direct comparison is made with the behaviour of the samarium analogue. Secondly, we have investigated the structure and properties of $Ba_{4.5}Nd_9Ti_{18}O_{54}$ when there was substantial replacement of Nd by Al, ie the system $(1-x)\ BaO \cdot Nd_2O_3 \cdot 4TiO_2 + x BaO \cdot Al_2O_3 \cdot 4TiO_2$. Here we are concerned predominantly with two phase products. For selected compositions, small amounts of Bi_2O_3 were also included in starting mixtures to assess whether densification or dielectric properties could be enhanced [7].

2. Experimental

All samples were prepared by the mixed oxide route. The starting materials were high purity (> 99.5%) powders of $BaCO_3$, Nd_2O_3, Bi_2O_3 and TiO_2 (Fluka Chemicals, UK) and Al_2O_3(Mandoval Ltd, grade AES-11C). Two primary base formulations were prepared: $Ba_{4.5}Nd_9Ti_{18}O_{54}$ (denoted as BNT) and $BaO \cdot Al_2O_3 \cdot 4TiO_2$ (denoted as BAT).

For the $Ba_{4.5}Nd_9Ti_{18}O_{54}$ base formulation, powders of $BaCO_3$, Nd_2O_3 and TiO_2 were combined in appropriate ratios to yield $Ba_{4.5}Nd_9Ti_{18}O_{54}$ after processing. The powders were ball milled (wet with propan-2-ol with zirconia media) for 16 hours, calcined at 1275°C for 4 hours. The aluminium end member ($BaO \cdot Al_2O_3 \cdot 4TiO_2$) was prepared in a similar manner using powders of $BaCO_3$, Al_2O_3 and TiO_2; after milling this powder mixture was calcined at 1050°C for 4 hours. Two series of samples were prepared:

1. when there was low doping of BNT by Al_2O_3: $Ba_{4.5}Nd_9Ti_{18}O_{54} + yAl_2O_3$ (where y = 0.0–1.0 wt %)
2. when there was a high level of replacement of Nd by Al, ie BNT-BAT system $(1-x)Ba_{4.5}Nd_9Ti_{18}O_{54} + x(BaO \cdot Al_2O_3 \cdot 4TiO_2)$,

For the investigation of Al doping of $Ba_{4.5}Nd_9Ti_{18}O_{54}$, appropriate amounts of Al_2O_3 (0.125, 0.25, 0.5, 0.75 and 1.0 wt%) were added to 50g batches of calcined $Ba_{4.5}Nd_9Ti_{18}O_{54}$. An additional batch having the composition $Ba_{4.5}Nd_9Ti_{18}O_{54}$ + 0.5 wt% Al_2O_3 + 8 wt%($Bi_2O_3 \cdot 2TiO_2$) was also prepared. These were wet milled for 24 hours, dried and pressed (at 100 MPa) into pellets of 10mm diameter, with lengths in the range 3–6 mm. Sintering was performed in oxygen at temperatures in the range 1200–1450°C for 4 h and cooled at 120°C/h.

For the investigation of the system BNT-BAT, powder batches of $(1-x)\ Ba_{4.5}Nd_9Ti_{18}O_{54} + x(BaO \cdot Al_2O_3 \cdot 4TiO_2)$ were prepared where x = 0.1, 0.2, 0.3, 0.4, 0.6, 0.8 and 1.0. The mixtures were wet milled for 6 hours, dried and calcined at temperatures at 1100° for $BaO \cdot Al_2O_3 \cdot 4TiO_2$ and $(1-x)Ba_{4.5}Nd_9Ti_{18}O_{54} + x(BaO \cdot Al_2O_3 \cdot 4TiO_2)$ and 1275°C for $Ba_{4.5}Nd_9Ti_{18}O_{54}$ for 4 hours. All mixtures were wet milled for 24 hours, then finally dried and pressed (at 100 MPa) into pellets of 10mm diameter with heights in the range 6–8 mm. Sintering was performed in oxygen at temperatures in the range 1200–1450°C for 4 hours and cooled at 120°C/hour.

Fired densities were determined by an immersion method. Calcined powders and sintered products were examined by X-ray diffraction (Philips X'PERT APD system) over a 2θ range of 20–60°. Lattice parameters were determined via a least square refinement of d-spacings data using CELREF program Version 3 [15]. Product morphologies were examined by optical and scanning electron microscopy (SEM); specimen surfaces were ground and polished down to $^1/_4\mu$m diamond paste and thermally etched at 1100–1200°C for 20 minutes. For SEM studies, specimens were carbon coated and examined using a Phillips 505 SEM, fitted with an EDAX 9100 energy dispersive spectroscopy (EDS) system. Selected samples were investigated by Transmission Electron Microscopy (TEM). Sintered pellets were crushed and ground in an agate mortar and pestle; the particles were deposited on a carbon coated copper grid. A Phillips EM430 Transmission Electron Microscope was used for lattice imaging and electron diffraction studies. Lattice images were obtained at accelerating voltage of 300 keV by the Many Beam Imaging (MBI) method.

Microwave dielectric properties were determined by the Hakki and Coleman dielectric resonator method [16]. The Temperature coefficient of resonant frequency (τ_f) measurements were performed using a silver plated aluminum cavity at temperatures between −10°C and +60°C

3. Results and Discussion

3.1. Al-Doped $BaO \cdot Nd_2O_3 \cdot 4TiO_2$ Ceramics

To densify undoped $Ba_{4.5}Nd_9Ti_{18}O_{54}$ ceramics, sintering temperatures above 1450°C are usually required [17]. When Al_2O_3 was added to the powder batches, it was found that the sintering temperature could be reduced by approximately 100°C. Roth et al. demonstrated that in the system BaO-Al_2O_3-TiO_2 a wide range of phases readily forms at 1275°C [18]. In this study good quality ceramics, with densities in excess of 5.5 g cm^{-3} ($\geq$ 95.6 % theoretical density), were obtained at temperatures in the range 1320–1400°C; there was minimal variation in density over this range. Figure 1 shows densities as a function of Al_2O_3 content for samples fired at 1350°C. The undoped ceramic has a very low density 4.75 g cm^{-3}, but ceramics prepared with alumina additions of 0.1–1.0 wt% exhibit universally high densities of approximately 5.6 g cm^{-3}

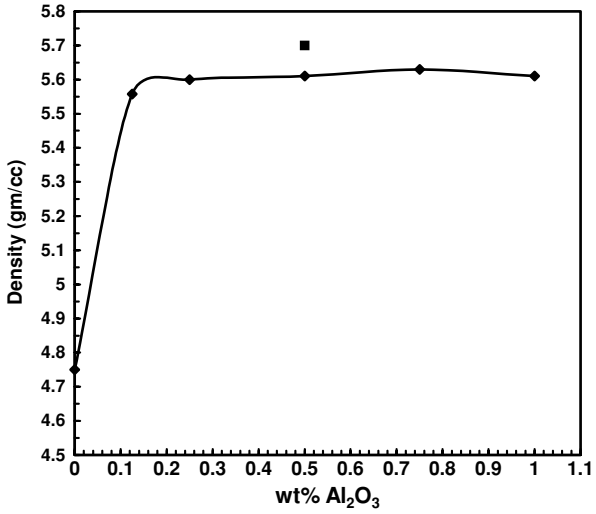

Fig. 1. Density of $BaO.Nd_2O_3.4TiO_2$ ceramic as a function of Al_2O_3 additions; samples sintered at 1350°C.

(∼97.4% theoretical). The single batch prepared with 0.5 wt% Al_2O_3 + 8 wt% Bi_2O_3 additions exhibited the highest density of 5.7 g cm^{-3}.

X-ray diffraction analysis indicated that all the samples prepared with 0.1–1.0 wt% Al_2O_3, sintered at temperatures of 1320°C - 1400°C, were single phase. The spectra (an example shown in Fig. 2) matched the accepted patterns for orthorhombic $Ba_{4.5}Nd_9Ti_{18}O_{54}$ [19]. The lattice parameters (Table 1) exhibited only limited variation with composition. As the amount of Al in the starting material increased, there was a net contraction of the b-axis and c-axis, and decrease in the cell volume. The reduction in volume reflects the incorporation of the smaller Al^{3+} ions (0.535 Å) in place of the larger Ti^{4+} ions (0.605 Å) and possibly the Nd^{3+} ions (1.04Å) [20]. The cell parameter changes are consistent with to those observed by Mizuta et al. [11] as Al substituted for Ti in the related tungsten bronze structured material $(Ba_{6-3x}Sm_{8+2x})_\alpha Ti_{18-y}Al_yO_{54}$.

Whilst all the undoped samples, and Al-containing samples fired at 1300°C or lower contained significant levels of porosity, the remaining specimens were of high density (≥97% theoretical) and exhibited uniform microstructures. Figure 3 shows a typical SEM micrograph. The grains are rounded to elongated in shape, 2–10μm in size, in random orientation. The incorporation of Al into the structure has minimal effect on the microstructure; Figure 3 is very similar to that for $Ba_{4.5}Nd_9Ti_{18}O_{54}$ prepared without Al additions

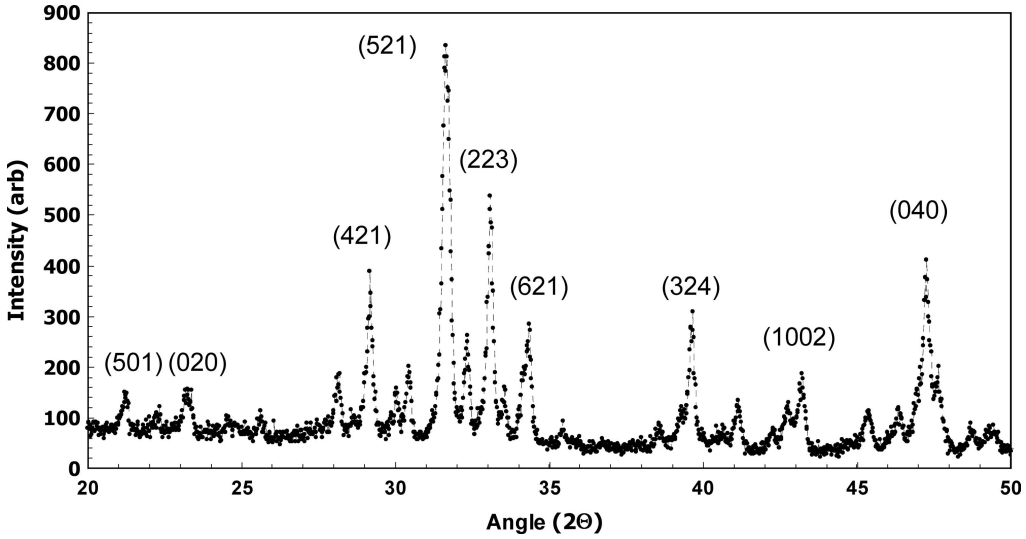

Fig. 2. Typical X-ray diffraction spectrum for $BaO \cdot Nd_2O_3 \cdot 4TiO_2$ ceramic prepared with Al_2O_3 additions up to 1 wt%.

[5]. EDS analysis revealed the presence of occasional, small, second phase grains, rich in Nd and Ti. There was no evidence of any second phase rich in Al. However the fact that the sintering temperature had been lowered (by typically 100°C) by Al_2O_3 additions, suggests that part of the Al could have been used to produce a low melting temperature phase [17], which aided sintering. High temperature dilatometry may be able to provide further information about the sintering mechanism.

The study of Ba-Sm-Al-Ti-O tungsten bronze structure ceramics by Mizuta et al. [11] demonstrated that small amounts of Al could be incorporated on the B site in place of Ti, $(Ba_{4.2}Sm_{9.2})_{1.044}Ti_{16.39}Al_{1.61}O_{54}$, ie up to 10% replacement of Ti^{4+} by Al^{3+}. Thus the remaining, indeed the bulk of the Al in the present study, is expected to be accommodated within the primary grains. EDS analysis of the grains suggests a maximum of ∼4% replacement of Ti by Al, with some Al substituting for Nd. This is consistent with the data that very small, occasional, second phase grains are rich in Nd and Ti. The latter grains were too small to enable reliable analysis. Substitution of Nd by Al is charge compensated. The replacement of Ti by Al leads to a reduction in positive charge. To enable charge balance it is anticipated that there could be generation of oxygen vacancies, for example two Ti^{4+} ions substituted by two Al^{3+} ions with the generation of an oxygen vacancy ($2Ti_{Ti}^{4+} \rightarrow 2Al_{Ti}^{3+} + O_v$), and perhaps coupling with the trace amounts of impurities. However, if vacancies are indeed generated, the fraction must be very small as the presence of Al in the lattice does not, initially, appear to have any serious deleterious effect on the dielectric losses (as will be demonstrated later).

Table 1. Lattice parameters of Al_2O_3 doped $BaO \cdot Nd_2O_3 \cdot 4TiO_2$ ceramics.

	Lattice parameters (±0.0005 Å)		
Al_2O_3 (Wt%)	a	b	c
0	22.3479	7.6955	12.2021
0.25	22.3442	7.6994	12.2036
0.5	22.344	7.6955	12.2079
0.75	22.3414	7.6962	12.2033
1	22.3418	7.6962	12.2005

Electron diffraction studies of the Al-containing ceramics confirmed an orthorhombic structure with a doubled unit-cell along the shortest axis. Figure 4 shows a HRTEM image along [10] for a sample prepared with additions of 0.5 wt% Al_2O_3 + 8 wt% $Bi_2O_3 \cdot 2TiO_2$. Similar images were obtained for other samples, and indeed Figure 4 is very similar to that obtained for $Ba_{4.5}Pr_9Ti_{18}O_{54}$ [21].

The dielectric properties of the Al-containing ceramics at microwave frequencies are presented in Figs. 5 and 6. Figure 5 shows the relative permittivity and

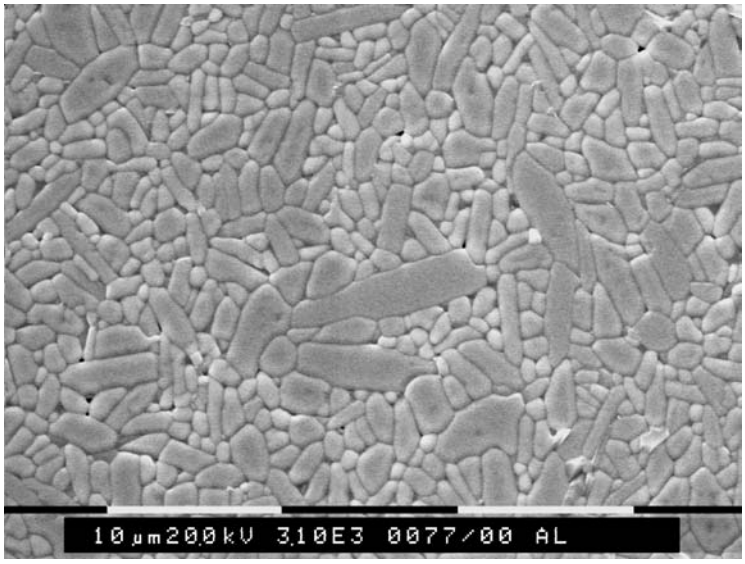

Fig. 3. SEM micrograph of $BaO \cdot Nd_2O_3 \cdot 4TiO_2$ ceramic prepared with 1 wt% Al_2O_3.

$Q \times f$ values as a function of Al content. From a maximum ε_r value of 88 there is a linear decrease in the relative permittivity with the increase of Al content. This trend is similar to that reported by Mizuta [11] for Al substitution in Ba-Sm-Ti-O solid solutions. The introduction of Al into the lattice can reduce the relative permittivity in two ways. Firsly it has lower polarisability, ie 0.79 Å^3 for Al^{3+} compared with 2.93 Å^3 for Ti^{4+} [22]. Secondly, the ionic radius of the substituting Al^{3+} ion (0.535 Å) is smaller than that of the

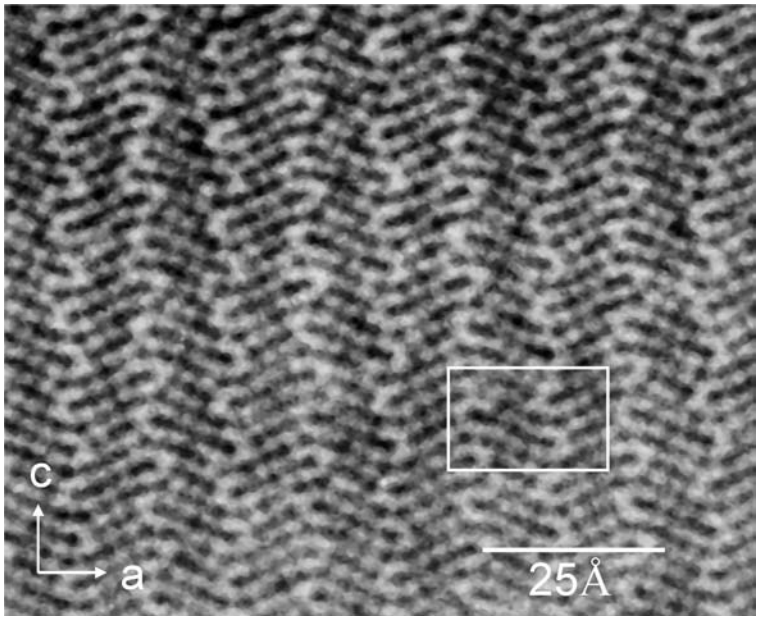

Fig. 4. High resolution TEM micrograph of $BaO \cdot Nd_2O_3 \cdot 4TiO_2$ ceramic prepared with 0.5 wt% Al_2O_3 plus 8 wt% Bi_2O_3. The rectangle shows the dimensions of the unit cell.

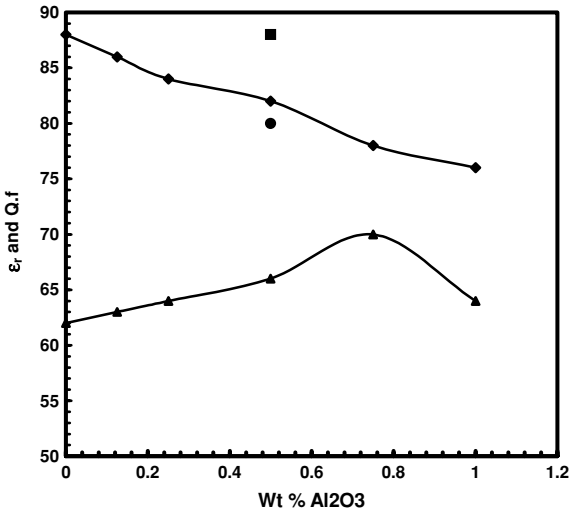

Fig. 5. Relative permittivity and $Q \times f/1000$ values for $BaO \cdot Nd_2O_3 \cdot 4TiO_2$ ceramics as a function of Al_2O_3 additions: ε_r of $BaO \cdot Nd_2O_3 \cdot 4TiO_2$ (♦); ε_r of $BaO \cdot Nd_2O_3 \cdot 4TiO_2$ + Bi_2O_3 (■); $Q \times f/1000$ of $BaO \cdot Nd_2O_3 \cdot 4TiO_2$ (▲); $Q \times f/1000$ of $BaO \cdot Nd_2O_3 \cdot 4TiO_2 + Bi_2O_3$ (●).

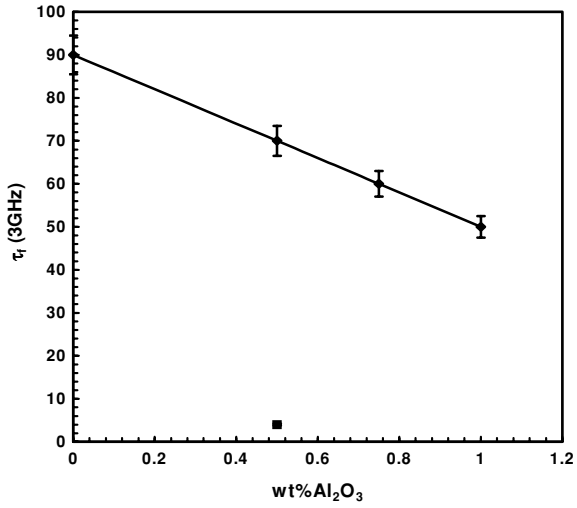

Fig. 6. Temperature coefficient of resonant frequency as a function of Al_2O_3 additions for: $BaO \cdot Nd_2O_3 \cdot 4TiO_2$ (♦); for $BaO \cdot Nd_2O_3 \cdot 4TiO_2 + Bi_2O_3$ (■).

host Ti^{4+} ion (0.605 Å) [11] and thus tends to reduce the size of the lattice by the contraction of the octahedra in the tungsten bronze framework. This has a direct effect on relative permittivity as demonstrated by Mizuta et al. [11]. For the addition of up to 1 wt% Al_2O_3 to $Ba_{4.5}Nd_9Ti_{18}O_{54}$ we also observed a small contraction in cell volume and infer that both mechanisms are relevant in the Nd-based system as well. On the basis of changes in the lattice parameters, microstructure and dielectric data we believe that solubility limit for Al in $Ba_{4.5}Nd_9Ti_{18}O_{54}$ is at least 0.35 mol%; (equivalent to ∼1 wt% Al_2O_3 additions). We surmise from the dielectric data (Fig. 5) that at least 80% of the Al enters the Ti sites. Substitution of significantly higher levels of Al led to the development of a two-phase microstructure and a dramatic reduction in ε_r, as will be demonstrated in Section 3.2.

The beneficial effect of Bi_2O_3 additions on the properties of $Ba_{4.5}Nd_9Ti_{18}O_{54}$ ceramics are well known [7]. The presence of Bi_2O_3 aids the sintering process, reduces sintering temperature and leads to the incorporation of some Bi into the primary structure. However, it is of interest to note that the combined additions of Al and Bi are particularly effective (Fig. 5), raising the relative permittivity back to the base line value of 88 and enhancing the $Q \times f$ values.

Figure 5 shows the Qf values as a function of Al content. In all cases the Qf values exceed 6000 GHz, and there is a slow steady increase from 6200 to 7000 GHz with increasing Al content up to 0.75 wt% Al_2O_3. This is in marked contrast to the findings of Mizuta et al. [11] for the effect of Al substitution in the system $(Ba_{6-3x}Sm_{8+2x})_\alpha Ti_{18-y}Al_yO_{54}$. They found that as y increased from zero to 1.6, there was a dramatic decrease in Qf values, with pronounced minima at $y = 0.5$ and $y = 1.3$. This was ascribed to the presence of vacancies at the A_2 sites, compensating for the decrease in positive charge upon Al substitution for Ti. This led to the very unusual effect of both ε_r and *Qf* decreasing as the level of Al substitution increased. In the Ba-Nd-Ti-O system investigated in the present study, the introduction of Al leads to a decrease in ε_r but an increase in *Qf* (i.e. ε_r is inversely proportional to *Qf*) that is more common. However, the one sample prepared with both Al_2O_3 and Bi_2O_3 additions yielded the highest *Qf* value, of approximately 8000 GHz. Whilst the presence of Bi_2O_3 aids sintering and microstructure development, a limited amount of Bi ions can be accommodated in the lattice [23], and this undoubtedly improves both ε_r and Qf values. It is believed that the Bi selectively enters one out three possible sites previously occupied by Nd [23].

Figure 6 shows the variation of τ_f with Al content. It is quite clear that the temperature coefficients of

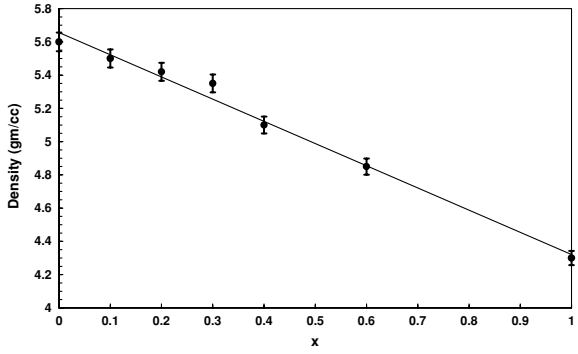

Fig. 7. Sintered density for samples in the system $(1 - x)BaO \cdot Nd_2O_3 \cdot 4TiO_2 + xBaO \cdot Al_2O_3 \cdot 4TiO_2$.

resonant frequency decreases with increasing Al content, reaching a value of 50 ppm/°C at 1 wt% Al_2O_3. From a practical point of view this is valuable as it provides a means of reducing or more specifically tuning τ_f to zero. The combined use of 0.5 wt% Al_2O_3 plus 8% Bi_2O_3 additions moved τ_f much closer to zero. No mechanism has been proposed for the modification of the dielectric properties by substitution of Bi in the crystal structure of $Ba_{4.5}Nd_9Ti_{18}O_{54}$ ceramics. However, it has been shown that Bi additions increase relative permittivity and move τ_f towards zero without degradation of the Q-values, within the solid solubility range (here approximately 2.4 mol % Bi is substituted for Nd sites [7]). After exceeding the solid solubility limit, additional Bi concentrates at the grain boundaries as a Bi-rich phase, causing considerable reduction of the Q-value and an increase in τ_f of such ceramics [11].

It is noted that there is considerable similarity in the data for the effect Al substitution on τ_f in both Ba-Sm-Ti-O [11] and Ba-Nd-Ti-O systems (this study). Mizuta et al. [11] tried to explain the reduction in τ_f upon Al substitution by a charge compensation mechanism, and by the effect of octahedral tilting [24]. The former was considered inadequate because of the magnitude of the change in τ_f, and thus a mechanism based on octahedral tilting [24] was favoured [11]. It would be of interest to investigate this proposal experimentally.

3.2. *Ceramics in the System $(1 - x)BaO \cdot Nd_2O_3 \cdot 4TiO_2$- $xBaO \cdot Al_2O_3 \cdot 4TiO_2$*

Ceramics prepared from powder mixtures based on $BaO \cdot Al_2O_3 \cdot 4TiO_2$ can readily be sintered to high density at temperatures as low as 1260°C. Such products are light grey in colour, but become progressively darker as the sintering temperature is increased to 1350°C. Fired densities are in the range 4.21 to 4.31gm/cc (equivalent to 97 to 99.5% theoretical). In the system $(1-x)(BaO \cdot Nd_2O_3 \cdot 4TiO_2)$—$x(BaO \cdot Al_2O_3 \cdot 4TiO_2)$, high density products were achieved after sintering at 1350°C (Fig. 7). There is an

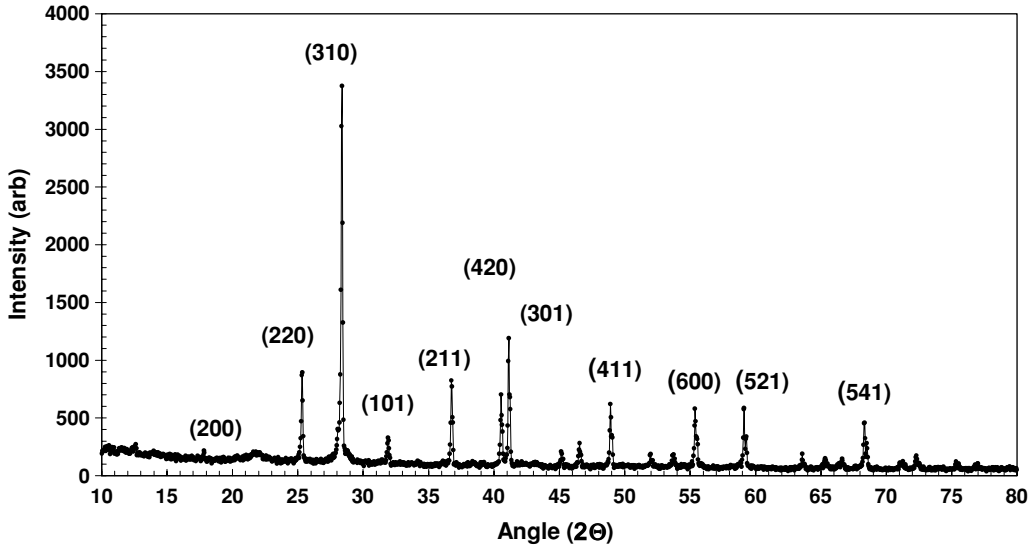

Fig. 8. X-ray diffraction spectrum for $BaO \cdot Al_2O_3 \cdot 4TiO_2$ ceramic.

almost linear, steady decrease in density as the heavier Nd ions are replaced by Al.

An X-ray diffraction spectrum for ceramic $BaO \cdot Al_2O_3 \cdot 4TiO_2$ is shown in Fig. 8. It is single phase, and all the peaks match that reported for $BaO \cdot Al_2O_3 \cdot 4.5TiO_2$ [14]. A phase diagram for BaO-Al_2O_3-TiO_2 at 1275°C shows a hollandite structure for $BaO \cdot Al_2O_3 \cdot 4TiO_2$ (ie 1:1:4.5), but there is an indication that the hollandite field should also incorporate the 1:1:4 composition, investigated here. On the basis of tetragonal symmetry, the lattice parameters were determined to be $a = 9.9491$ Å and $c = 2.9254$ Å.

Typical SEM micrographs for $BaO \cdot Al_2O_3 \cdot 4TiO_2$ and $0.2(BaO \cdot Al_2O_3 \cdot 4TiO_2) - 0.8(BaO \cdot Nd_2O_3 \cdot 4TiO_2)$ are presented in Fig 9. Whilst there is evidence of needle-like grains (similar to that for $BaO \cdot Nd_2O_3 \cdot 4TiO_2$, shown in Fig. 3) the microstructure of the Al end member ($BaO \cdot Al_2O_3 \cdot 4TiO_2$;

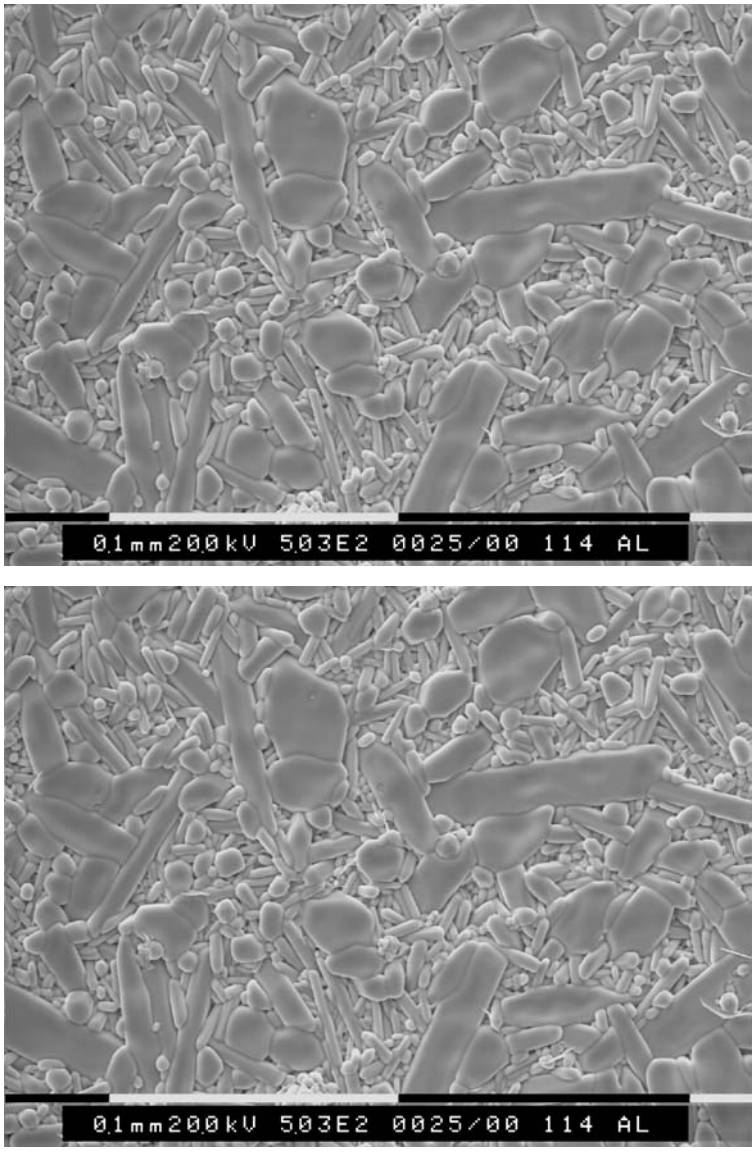

Fig. 9. SEM micrographs of (a) $BaO \cdot Al_2O_3 \cdot 4TiO_2$, (b) $0.8BaO \cdot Nd_2O_3 \cdot 4TiO_2 + 0.2BaO \cdot Al_2O_3 \cdot 4TiO_2$. Grains rich in $BaO \cdot Al_2O_3 \cdot 4TiO_2$ denoted by *A*; grains rich in $BaO \cdot Nd_2O_3 \cdot 4TiO_2$ denoted by *N*.

Figure 9(a)) is dominated by lath shaped grains up to 80 μm in size. In addition there is significantly greater variability in grain size than in Fig. 3. For mixed compositions, such as $0.2(BaO \cdot Al_2O_3 \cdot 4TiO_2)$–$0.8(BaO \cdot Nd_2O_3 \cdot 4TiO_2)$, Fig. 9(b), there are clear microstructural characteristics of the Al and Nd end members; there are both needle-like grains (rich in Nd) and large, rounded lath-shaped grains (rich in Al). Detailed EDS examination confirmed that the two phases were essentially $BaO \cdot Nd_2O_3 \cdot 4TiO_2$ and $BaO \cdot Al_2O_3 \cdot 4TiO_2$ with very limited evidence of the solubility of one in the other. Whilst the shapes of the grains of the two individual phases (Fig. 9(b)) are virtually the same as in the two end-members (Figs. 3 and 9(a)), grains of the $BaO \cdot Al_2O_3 \cdot 4TiO_2$ phase were smaller in the mixed phase samples, eg up to 40 μm long in the $0.8(BaO \cdot Nd_2O_3 \cdot 4TiO_2) + 0.2(BaO \cdot Al_2O_3 \cdot 4TiO_2)$ composition, but 80 μm in the $BaO \cdot Al_2O_3 \cdot 4TiO_2$end member. In the mixed phases, the amount and size of the $BaO \cdot Al_2O_3 \cdot 4TiO_2$ grains tended to increase as the Al content in the system increased. This appears to reflect the fact that the $BaO \cdot Al_2O_3 \cdot 4TiO_2$ phase can be sintered at significantly lower temperatures than the $BaO \cdot Nd_2O_3 \cdot 4TiO_2$ phase.

Figure 10 shows the ε_r and $Q \times f$ values for the $(1-x)$ $BaO \cdot Nd_2O_3 \cdot 4TiO_2 - xBaO \cdot Al_2O_3 \cdot 4TiO_2$ ceramics. Although the Al end member exhibits modest relative permittivity and $Q \times f$ values, many of the mixed phase compositions exhibit significant improvement in $Q \times f$ values over the conventional Nd end member. Indeed for compositions containing 0.10-$0.60(BaO \cdot Nd_2O_3 \cdot 4TiO_2)$ the $Q \times f$ values are all in excess of 6200 (the value of the Nd end member) and there is a peak $Q \times f$ value of ~9000 2GHz at $x = 0.2$. With increasing Al content in the system, ε_r decreases from 88 (in $BaO \cdot Nd_2O_3 \cdot 4TiO_2$) to approximately 35 in the Al end member. However, relative permittivities in excess of 65 are achieved in mixed compositions containing $\leq$0.2 ($BaO \cdot Al_2O_3 \cdot 4TiO_2$). Figure 11 demonstrates that the Nd and Al end members exhibit $\tau_f$values of opposite polarity; τ_f is + 90 ppm/°C in $BaO \cdot Nd_2O_3 \cdot 4TiO_2$ but –14 ppm/°C in $BaO.Al_2O_3 \cdot 4TiO_2$. The variation in τ_f is grossly non linear, with the greatest change in values from $0 \leq \times \leq 0.2$. From a practical point of view this is the most important region as τ_f passes through a zero value around x = 0.14. It is interesting to note that at this composition (Fig. 10) the relative permittivity is approximately 71, and the $Q \times f$ value approximately 8200 GHz. Thus the mixed compositions containing up to 20% replacement of Nd by Al, exhibit an attractive combination of dielectric properties, generally superior to those of the undoped $BaO \cdot Nd_2O_3 \cdot 4TiO_2$ end member. For compositions in which $0 \leq x \leq 0.2$ the Al solubility limit for $BaO \cdot Nd_2O_3 \cdot 4TiO_2$is greatly exceeded and individual grains of $BaO \cdot Al_2O_3 \cdot 4TiO_2$ will have started to form. However, the microstructure and properties are still dominated by the Nd end member, although the benefit of superior sinterability and near zero τ_f are realised through the growing Al content. Why the $Q \times f$ values in the mixed compositions ($0.1 \leq$ x ≤ 0.5) should be so much higher than in either of the two end members is not entirely clear, but this preliminary survey of the $(1-x)$ $BaO \cdot Nd_2O_3 \cdot 4TiO_2$-$xBaO \cdot Al_2O_3 \cdot 4TiO_2$ has demonstrated that the system is worthy of further investigation.

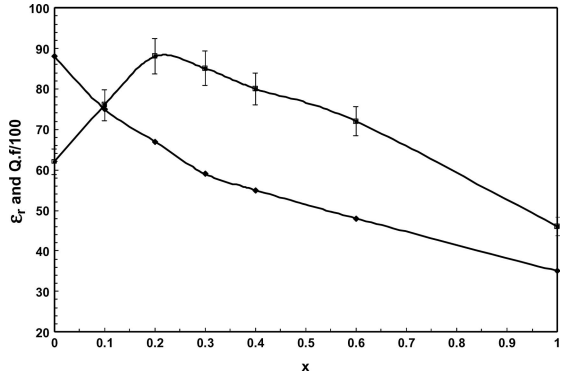

Fig. 10. Relative permittivity and $Q \times f/1000$ values for $(1-x)BaO \cdot Nd_2O_3 \cdot 4TiO_2 + xBaO \cdot Al_2O_3 \cdot 4TiO_2$ ceramics as a function of x: ε_r (♦); $Q \times f/1000$ (■).

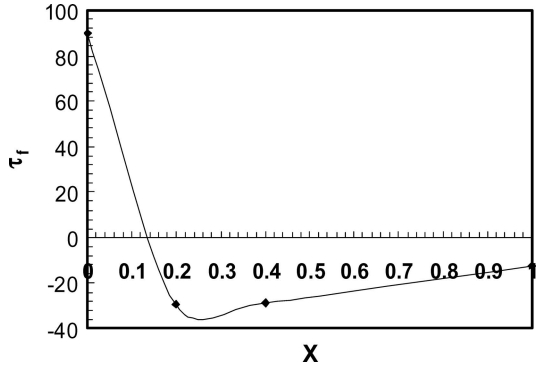

Fig. 11. Temperature coefficient of resonant frequency for $(1-x)BaO \cdot Nd_2O_3 \cdot 4TiO_2 + xBaO \cdot Al_2O_3 \cdot 4TiO_2$ ceramics as a function of x.

4. Conclusions

The addition of up to 1 wt% Al_2O_3 to $BaO \cdot Nd_2O_3 \cdot 4TiO_2$ yielded high-density ceramics with a needle-like microstructure, and no evidence of a second phase. Very small amounts of Al (up to 0.35 mol%) can be accommodated into the Ti octahedra. This leads to a reduction in ε_r values (as a result of lower polarisability and ionic radii for Al^{3+} compared to Ti^{4+}), but an increase in $Q \times f$ values to over 8000 GHz. The presence of Al within the structure reduces the temperature coefficient of resonant frequency from 90 ppm/°C to approximately 60 ppm/°C. It is well established that Bi_2O_3 can improve the sinterability and properties of tungsten bronze structure microwave dielectrics. In the present $BaO \cdot Nd_2O_3 \cdot 4TiO_2$ ceramics prepared with additions of 0.5 wt% Al_2O_3 and 8 wt% Bi_2O_3 exhibited improved densification, higher ε_r and $Q \times f$ values, but lower τ_f values (nearer zero).

Additions of large amounts of Al_2O_3 to $BaO \cdot Nd_2O_3 \cdot 4TiO_2$ led to a reduction in the sintering temperature and the development of a two-phase microstructure because of the very limited solid solubility. The end member $BaO.Al_2O_3 \cdot 4TiO_2$ is characterised by large lath shaped grains up to 80 μm in size. Mixed Al-Nd ceramics contain both needle shaped (Nd rich) grains and lath shaped (Al-rich) grains, but of smaller dimension than in the Al end member. The dielectric properties of the mixed system are optimised at compositions near $x = 0.14$, i.e. $\sim$16% replacement of Nd by Al; the $Q \times f$ value is increased to 8200 GHz, the ε_r suffers a small reduction to 71, but τ_f is tuned to very close to zero ppm/°C.

Acknowledgments

The financial support of EPSRC through the Grant GR/L33306 is gratefully acknowledged.

References

1. T Negas and P. Davies, *Ceram. Trans*., **53** , 179 (1995).
2. D. Kolar, Z. Stadier, S. Gaberscek and D. Suvorov, *Ber. Deut Keram. Ges.*, **55**, 366 (1978).
3. E.A. Nenasheva, B.A. Rotenber, E.I. Gindin, and V.G. Prokhvatilov, *Neorg. Mater*., **15**, 1890 (1979).
4. H. Ohsato, S. Nishigaki, and T. Okuda , *Jpn. J. Appl. Phys.*, **31**, 3136 (1992).
5. F. Azough, R. Freer, P. Setasuwon, C. Leach and P. Smith, *Ceramic Transactions*, Vol. 100, edited by K.M. Nain and A.S. Bhalla (American Ceramic Society, Westerville, OH, 1999), p.257.
6. K. Wakino, K. Minai, and H. Tamura, *J. Am. Ceram. Soc.*, **67**, 278 (1984).
7. M. Valent, D. Suvorov, and D. Kolar, *J. Mater. Res.*, 11, 928 (1996).
8. R.G. Matveeva, M.B. Varfolomeev, and L.S. Il'yushenko, Trans. from *Zh. Neorg Khimi*., **29**, 31 (1984).
9. J.P. Guha and D. Kolar, *J. Am. Ceram. Soc.*, **55**, 55 (1972).
10. R. Ubic, I.M. Reaney, and WE Lee, *Int Mater Revs*, **43**, 205 (1998).
11. Mizuta, K. Uenoyama, H. Ohsato, S. Nishigaki and T. Okuda, *Jpn. J. Sol. State Phys*., 35 5065 (1996).
12. J.P. Guha, D. Kolar and B. Volavsek, *J. Solid State Chem.*, **16**, 49 (1976).
13. A.G. Solomah, R. Odoj and C. Freiburg, *J. Am. Ceram. Soc.*, **66**, c182 (1983).
14. JCPDS File No. 33-0133.
15. U.D. Altermat and I.D Brown, *Acta Cryst*, **A43**, 125 (1987).
16. B.W. Hakki and P.D. Coleman, *IEEE Trans. Microwave Theory*, **MTT-18**, 402 (1980).
17. P. Setasuwon, Ph. D thesis, University of Manchester (1995).
18. R.S. Roth, W.S. Brower, M. Austin, and M. Koob, Natl Bur Stand Tech Rep NBSIR (US) Report 81-2441, (NBS, Gaithesburg, Maryland, 1981) p.42; also in Phase Diagrams for Ceramists, Fig EC-415.
19. C.C. Tang, M.A. Roberts, F. Azough, C. Leach, and R. Freer, *J. Mater. Res.*, **17**, 675 (2002).
20. R.D. Shannon, *Acta Cryst*, **A32**, 751 (1976).
21. F. Azough, A.C. Wright, and R. Freer, *J. Mater. Sci.*, **36**, 5093 (2001).
22. R.D. Shannon, *J Appl Phys*, **73**, 348 (1993).
23. M. Valent, I. Arcon. D. Suvorov, A. Kodre, T. Negas, and R. Frahm, *J. Mat. Res.*, **12**, 799 (1997).
24. J. Joseph, T.M. Vimala, K.C. Raju, and V.R.K. Murthy, *Jpn. J. Appl. Phys.*, **35**, 179 (1996).